# Laser Peening Induced Shock Waves and Cavitation Bubbles in Water Studied by Optical Schlieren Visualization

L. Martí-López[a,b], R. Ocaña[a,]*, E. Piñeiro[c], A. Asensio [c]

[a]*Dept. Láser, Asociación Industrial de Óptica, Color e Imagen. Nicolás Copérnico 7, Parque Tecnológico de Valencia, 46980, Valencia, Spain*
[b]*Centro de Aplicaciones Tecnológicas y Desarrollo Nuclear, Calle 30 no. 502 esquina a 5ta Avenida, Miramar, Playa, La Habana, Cuba*
[c] *Centro de Aplicaciones Láser, Asociación de Investigación Metalúrgica del Noroeste, Relva 27, 36410 O Porriño, Pontevedra, Spain*

**Abstract**

A temporal and spatial study of the dynamics of generated shock waves and cavitation bubbles in water by laser peening using nanosecond Nd:YAG laser pulses is reported. False schlieren photographs of the zone surrounding the laser spot on the target were recorded by a fast ICCD camera. The developed experimental setup allowed us to obtain a visualization of the different phenomena (hemispherical, cylindrical and plane shock fronts, cavitation bubbles, phase disturbance tracks, plasma formation, etc.) that occur after the arrival of the laser pulse and that contain valuable information about the mechanical processes that take place on the sample.

*Keywords:* Laser peening, laser shock processing, schlieren, shock waves, cavitation bubble

## 1. Introduction

Laser processing of materials in liquid media has been gaining importance in recent years [1]. Among the most promising applications one can mention laser peening (also called laser shock processing) [2, 3], nanoparticle synthesis [4] and shock-wave laser cleaning [5]. Furthermore, many laser medical procedures can be explained in first approximation as processes taking place in aqueous media since human tissues contain a high percent of water (see, for example, [6, 7]). These characteristics encourage the investigation of the interaction high-power laser beam/liquid medium/target material.

Regarding laser peening, most research reports are devoted to the study of the relationship of the laser beam parameters (pulse energy, mean radiant exposure, spot diameter, pulse width, number of pulse per unit of area, etc.) with the obtained mechanical properties of the processed surface (for example, fracture toughness, micro hardness, wear and friction behavior and compressive residual stress). However, only in few works [8], the physical phenomena that appear after the arrival of the laser pulse are investigated. We also note that many published works on laser-induced shock waves and cavitation bubbles in water near metal surfaces do not explore the conditions of the laser peening technique (see for example [9-11]) and however it seems that only a few experimental data

* Corresponding author. Tel.: +34 96 131 80 51.
 *E-mail address*: rocana@aido.es.

regarding laser ablation underwater do present similarities with the conditions of the laser peening (see for example, [12-14]).

The aim of this work is hence to present a systematic study of the phenomena that appear as consequence of the surface treatment by laser peening in order to gain knowledge of the physical processes involved. To this end, we have recorded false schlieren photographs (without using a sharp edge) of the zone surrounding the impact place of single laser pulses on a Marlok maraging steel sample. The results allow us to identify different occurring phenomena such as hemispherical, cylindrical and plane shock fronts, cavitation bubbles, phase disturbance tracks, and plasma formation.

## 2. Experimental Setup

The developed optical set-up is shown in Figure 1. The component blocks of the optical set-up are described in the caption of the figure and as follows:
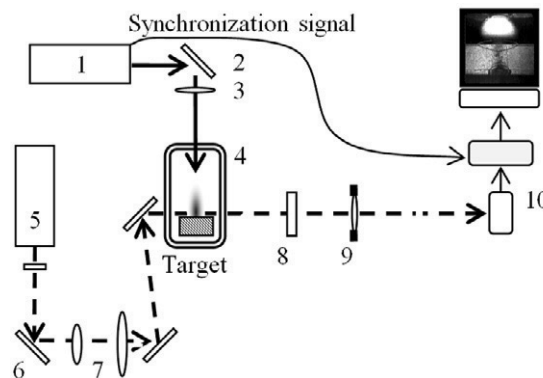


Figure 1. Simplified scheme of the optical set-up. 1) Laser, (2) 100% mirror, (3) lens f=200 mm, (4) tank, (5) laser + safety shutter, (6) 100% mirror, (7) beam expander, (8) spectral filter, (9) lens f=150 mm, and (10) ICCD + frame grabber + PC.

1. Laser shot block. The Q-switched Nd:YAG laser 1, Quanta-Ray PRO 290, Spectra-Physics) delivers light pulses of 1.4 J ± 0.1 J with a wavelength of 1.064 μm and FWHM width of 8 ns to mirror 2,which reflects them to lens 2 (f = 200 mm). This lens focuses laser pulses on a Marlok maraging steel sample (dimensions, 20 mm × 30 mm× 90 mm). The estimated beam diameter on the sample surface is 0.3 mm. The tank 4 (dimensions: 143.5 mm × 75.0 mm × 67.3 mm) filled with deionized water at 25 °C, is made of polyvinyl chlorine (PVC), and has 4 BK-7 optical quality windows (one frontal, two lateral, and one rear, not shown in Figure 1). This allows the probe beam to pass through the tank and the pulsed beam to reach the surface of the sample in the horizontal plane (parallel to Figure 1). When designing, tank dimensions have been chosen so that sound waves reflected from the front and the lateral windows get back to the pulse impact place on the target after approximately 90 μs and 23 μs, respectively (for this estimation it has been assumed that the sound speed in water is 1509 m/s at room temperature and atmospheric pressure, see ref. [15]).

2. Laser probe block. Laser (5) is a CW diode pumped frequency-doubled Nd:YAG laser (model MGH-F from Changchun New Industries, λ = 532 nm, P = 1,2 W. Probe beam is reflected by mirror 6, and expanded to a diameter of about 50 mm by beam expander 7. After reflecting by two mirrors that are used for fine alignment purposes, the beam passes through one of the lateral windows of the tank, illuminates the interaction zone, and leaves the tank through the other lateral window. The spectral filter 8 (center wavelength λ = 532 nm, FWHM bandwidth 2 nm for the frequency-doubled Nd:YAG laser), transmits with low losses the probe beam and blocks most of the light emitted by the plasma)

3. Imaging block. It is composed of a spatial filter (8), a lens (9, f = 150 mm, diameter = 20 mm), and an intensified CCD (ICCD) array (13, model DH734-18U-03, 1024 pixels × 1024 pixels, from Andor). Alternatively

we also used a fast streak camera model APX 250 RS able to capture video at 25000 frames per second and a Pentax 90x. The synchronization signal from the Q-switch allows fine adjustment of the delay between laser pulse and image capture. The magnification M of the imaging system can be varied easily from M = −1/4 to 5 by displacing the lens along the beam direction.

## 3. Results and Discussion

In order to review the physical phenomena that take place on the sample in water after the arrival of the laser pulse, we firstly provide a general description of the main effects that occur without considering the first interface that the laser beam finds when approaching the sample (either a double air-window-water interface at the tank in case of horizontal incidence or air-water in case of vertical incidence). Next, we discuss important aspects for the laser peening process such as the influence of the thickness of the water layer, the maximum shot peening frequency, the luminescence and the degassing of water.

### 3.1. Optical breakdown, hemispherical shock wave, acoustic wave planes, V shaped phase disturbances, and cavitation bubble

In Figure 2 we show a false schlieren image of the sample in water at $t$ =1 μs (i.e. 1 μs after the arrival of the laser pulse). The image has been taken from a previous experiment reported in ref. [16]. Conclusions can be summarized as follows. First, the incident laser pulse generates a line of mini blasts due to optical breakdown. Due to the superposition of spherical shock fronts emitted from each mini blast, a cylindrical shock front is formed (6). The radial speed of the cylindrical wave front is about 8400 m/s measured at $t$ = 40 ns and 9.1 mm away from the sample surface. Later ($t$ >> 100 ns) the radial speed diminishes to sound speed in water at atmospheric pressure. Inside the cylindrical shock front there is a zone of radial-graded optical path and a cluster of severe phase disturbances (the phase disturbance track)(7). This track vanishes almost completely at approximately $t$ = 1ms.

Second, a hemispherical shock front leaves the sample from the laser spot site (5). The speed of the hemispherical wave front is about 3700 m/s at $t$ = 200 ns and decreases to sound speed in water at $t$ >> 200 ns.

Third, the laser shot excites trains of acoustic plane waves in the water (3). The first one is emitted simultaneously (within the experimental uncertainty) with the hemispherical shock front. The following wave fronts emerge from the sample surface after multiple reflections of the acoustic wave inside the sample. Hence, the sound speed in the sample can be derived using a simple model. The result suggests that the acoustic wave inside the sample is mainly longitudinal.

Fourth, a cavitation bubble arises after the hemispherical shock wave (4), undergoes cycles of expansion and contraction and finishes its life as a bunch of small bubbles that ascends to the water surface at approximately $t$ = 15ms.

Fifth, we found V shaped phase disturbances that propagate on both sides of the hemispherical shock front, with their vertices hidden inside it (2). Such phase structures are the result of complex hydrodynamic phenomena. Further experiments are needed to clarify their origin and properties.
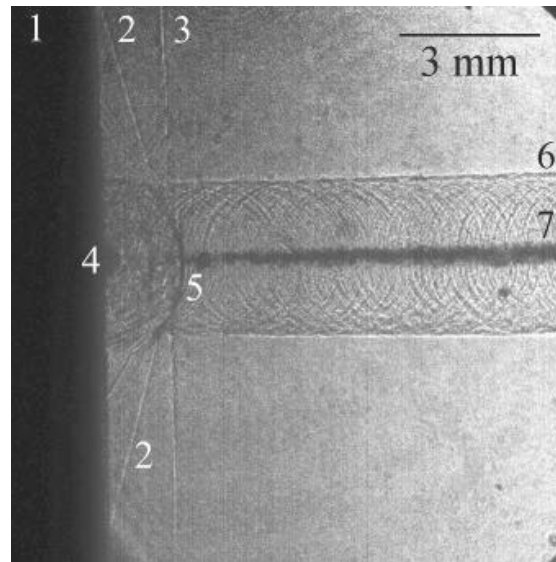
Figure 2. False schlieren picture of the sample in water 1000 ns after the arrival of the laser pulse. 1) Sample, (2) V shaped optical disturbances, (3) plane wave front moving away from the sample, (4) a cavitation bubble at the initial stage of expansion, (5) hemispherical shock wave, (6) the wave front resulting from the superposition of spherical shock waves due to optical breakdown, and (7) track of optical disturbances.

## 3.2. Influence of the thickness of the water layer

The laser peening process typically employs a curtain of water flowed over the workpiece, to confine and redirect the process generated shock waves into the bulk of the material and hence to create beneficial compressive residual stresses. We have carried out a systematic study of the thickness of the water layer to illustrate this property and gain knowledge about the increase of the shock wave peak pressure as function of the water layer. Figure 3 shows a series of schlieren images taken at fixed time delay $t = 400$ ns for different thicknesses of the water layer. As the thickness of the water layer decreases, the radii of the hemispherical shock wave and those of the cavitation bubbles increase. This fact indicates that the peak pressure exerted on the sample also increases.
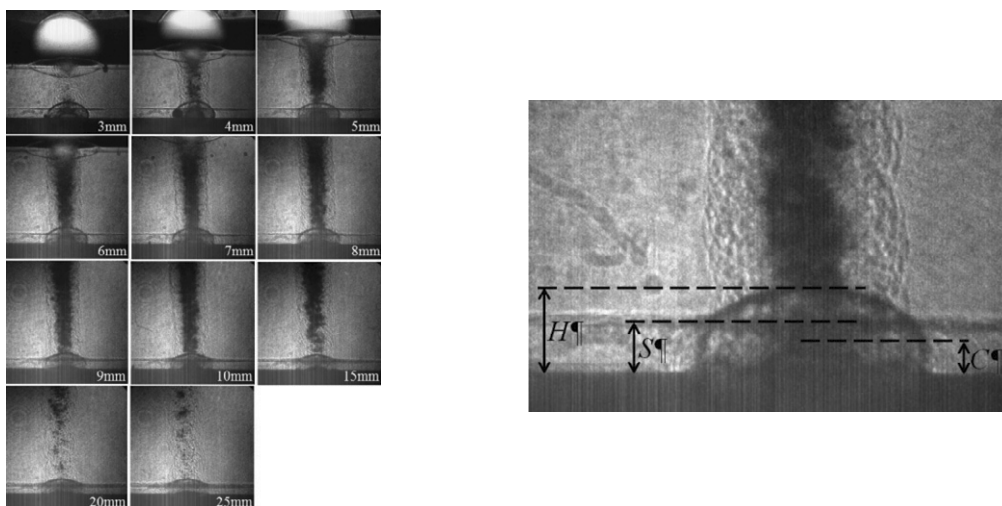


Figure 3. Left: false Schlieren pictures of zone surrounding the laser spot for different thicknesses of the water layer and constant delay time t = 400ns. Water layer thickness is indicated at the bottom of each image. Right: Measured parameters, where H denotes the radius of the hemispherical shock wave, S the position of the acoustic plane wave and C the radius of the cavitation bubble.

To characterize this effect we measured the radius $H$ of the hemispherical shock wave, the position $S$ of the acoustic plane wave and the radius $C$ of the cavitation bubble. In Figure 3 these parameters have been illustrated. The dependences of $H$, $S$ and $C$ as function of the thickness of the water layer are shown in Figure 4
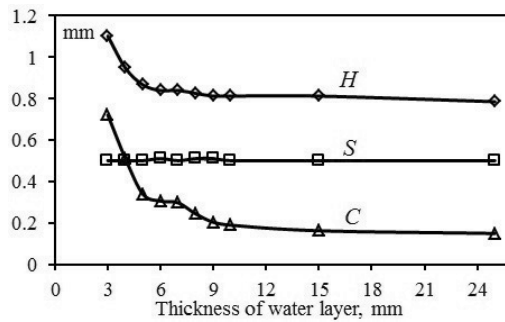


Figure 4. Radius of the hemispherical shock wave H, position of the acoustic plane wave S and radius of the cavitation bubble C at t = 400ns.

From Figure 4 it can be concluded that the speed of both shock wave and cavitation bubble increases substantially when the thickness of the water layer is reduced. Let us now estimate the increment of the shock wave peak pressure. For a spherical shock wave in a liquid, the difference peak pressure minus pressure behind the wave front is given by the following expression

$$\Delta P = P - P_0 = \frac{\rho_{02} v(v - v_s)}{m},\tag{1}$$

where P is the peak pressure, $P_0$ is the pressure behind the shock wave, $\rho_{02}$ is the density of the medium, $v_s$ is the sound speed ($v_s \approx 1500$ m/s for water at 30°C and atmospheric pressure), and m is an empirical coefficient (m = 2.1 for water). Expression (1) can be derived from the second Newton law linking peak pressure and shock wave speed. Now the pressure difference corresponding to two layers with thickness 3 mm and 4 mm can be written as follows:

$$\Delta P_{H=3mm} = \frac{v_{H=3mm}(v_{H=3mm} - v_s)}{v_{H=4mm}(v_{H=4mm} - v_s)} \Delta P_{H=4mm}\tag{2}$$

From the curves of Figure 4 we can estimate the speeds $v_{H=3mm}$ and $v_{H=4mm}$. It yields:

$$v_{H=4mm} \sim 1.9 v_s, \ \ v_{H=3mm} \sim 1.16 v_{H=4mm},\tag{3}$$

Substituting these values into expression (2) we obtain:

$$\Delta P_{H=3mm} \sim \frac{1.16(1.16 \times 1.9 - 1)}{0.9} P_{H=4mm} = 1.6 P_{H=4mm}.\tag{4}$$

Thus, the pressure difference increases about 60%.

### 3.3. Maximum shot peening frequency

The maximum repetition rate determines the productivity of the laser shot processing. A simple way to obtain an estimation of the maximum repetition rate is by inspecting a series of photographs of the process. Figure 5 shows nine false schlieren photographs of the surroundings of the laser spot with a thickness of water layer of 5mm. Water jets and associated splashes appear at t ~ 18µs and repeat several times. At early times splash is associated with collisions of shock waves and cavitation bubbles coming from the sample and from the air/water interface. During those collisions sudden mass transfers occur due to the pressure differences.
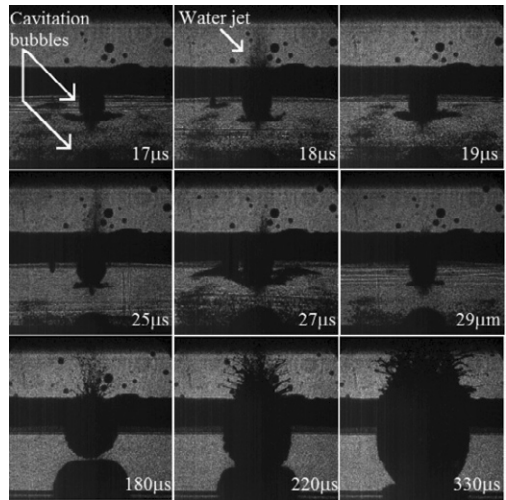
Figure 5. Early water jets. Thickness of water layer 5mm.

Figure 6 contains twelve schlieren photographs recorded at late times (dozens of ms). The voids of the water layer can be clearly observed.
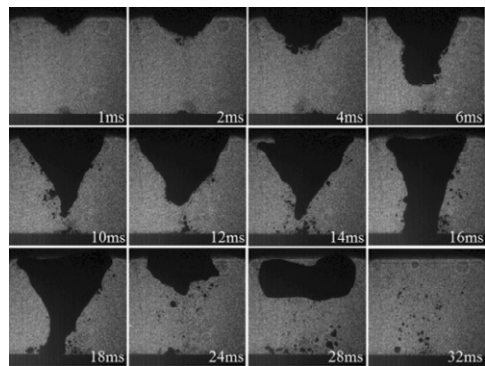


Figure 6. Volume effects of laser pulses. Thickness of water layer 10mm.

Figure 7 shows six images of the splash after arrival of the laser pulse. The main contribution to the splash effect is the upward jet occurring at 12 ms − 30 ms, which is followed by upward traveling drops. Splashing finishes at approximately 166 ms.
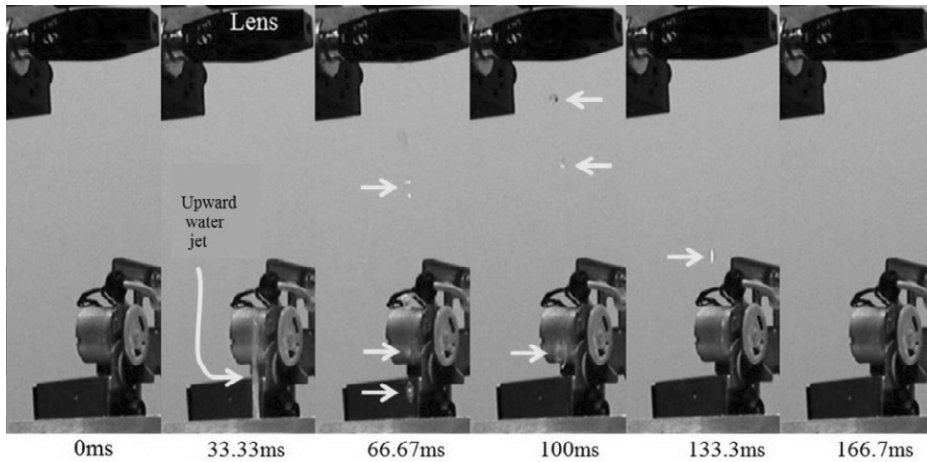


Figure 7. Water jet and splash following the laser pulse. The short yellow arrows mark the water drops that are expulsed from the water surface (bottom of the images). Thickness of the water layer 3mm

Let us estimate the maximum repetition rate of the laser pulses for the conditions of our set-up. When no special measures are taken into account to eliminate splashing, the minimum time interval between two consecutive laser pulses is determined by the duration of the splashing . Since that interval is ~ 166 ms, the maximum repetition rate is ~ 6 Hz. If splashing is controlled in some way, the minimum time interval is entirely determined by duration of the water voids and, hence the maximum repetition rate is ~ 30 Hz.

### 3.4. Luminescence

Figure 8 contains a sequence of false schlieren photographs that illustrate plasma formation during the first 110 ns. In the focal zone, the optical breakdown leads to formation of plasma accompanied by luminescence. Luminescence at the sample surface starts at $t \approx 40$ ns, reaches a maximum at $t \approx 45 - 50$ ns and vanishes at $t \approx 80$ ns. The luminescence at the air/water interface starts 5ns later and lasts much longer. Notice also that the luminescence of the beam track starts at $t \approx 45$ ns, and it is difficult to resolve it at larger delays. To clarify the behavior of the luminescence we have recorded a series of photographs of the laser spot zone with no interferential filter, blocking laser probe beam (note that they are not schlieren photographs) and at 22° incidence angle. The reason for the incidence angle is described in the following. In fact, different scenarios could explain the luminescence at the air/water interface (see Figure 8). For example, a strong ionization caused by ultraviolet radiation coming from the plasma at sample surface, could initiate processes leading to luminescence at the air/water interface. In such a case, luminescence would be centered in the vertical line over the laser spot on the sample. Another possible scenario might be explained in terms of the "moving breakdown" model described by Docchio et al. [17]. If the latter case takes place, we could expect that the luminescence does not occur in the vertical line over the laser spot on the sample, but at the entrance zone of the laser pulse into the water.
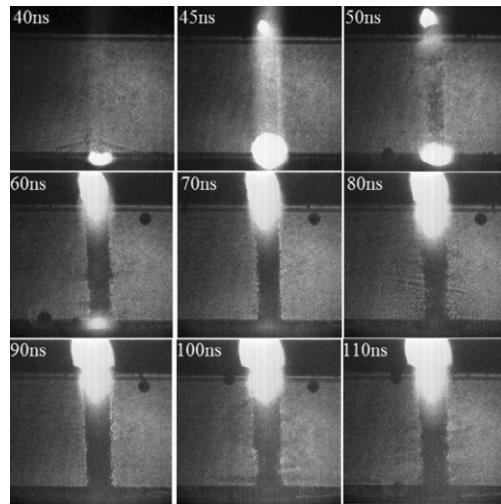
Figure 8. Plasma formation during the first 110 ns. Conditions of the experiment: thickness of water layer 5mm, ICCD gain 100, incidence angle 0°.

In Figure 9 we show obtained photographs with the laser beam at an angle of incidence of 22 degrees. It seems that the first of above described scenarios at early times is likely to occur.
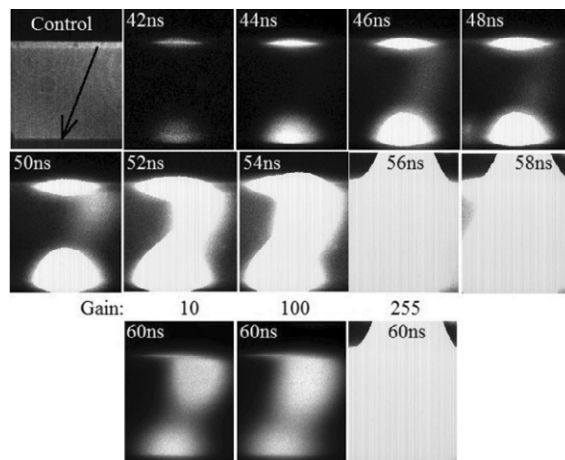


Figure 9. Plasma formation during the first 60 ns. Conditions of the experiment: thickness of water layer 4mm, incidence angle 22° (the arrow in the control photograph shows the direction of the beam), probe beam blocked (except for the control photograph). Photographs of the first two rows were recorded with an ICCD gain of 255. The images of the third row show the effect of increasing ICCD gain for a delay time t = 60ns.

Figure 10 shows a series of photographs recorded at relatively late times. It seems that air/water interface luminescence lasts about 2000 ns.
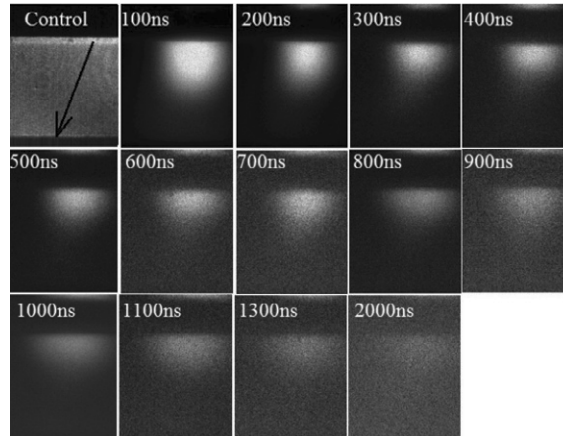


Figure 10. Late-time behavior of the plasma. Conditions of the experiment: thickness of water layer 4mm, incidence angle 22° (the arrow in the control photograph shows the direction of the beam), probe beam blocked (except for the control photograph). Photographs of the first two rows were recorded with an ICCD gain of 255

### 3.5. Water degassing

We have tested the effect of degassing water for the laser shock processing [18]. To degas deionized water we boiled it for 10 minutes at atmospheric pressure. The boiled water was kept in an airtight flask with no air inside. During the experiments, degassed water was maintained at room temperature. We carried out two series of shots: a series with degassed water and a control series with non-degassed water for comparison purposes. Figure11 shows the cavitation bubbles occurring in non-degassed and degassed water. Within the uncertainty of our experiments we did not detect a substantial increase of the speed of shock waves or of the radius of cavitation bubbles due to degassing. This result suggests that degassing has no influence in the dynamics of the shock waves and cavitation bubbles for the conditions of the laser shock processing.
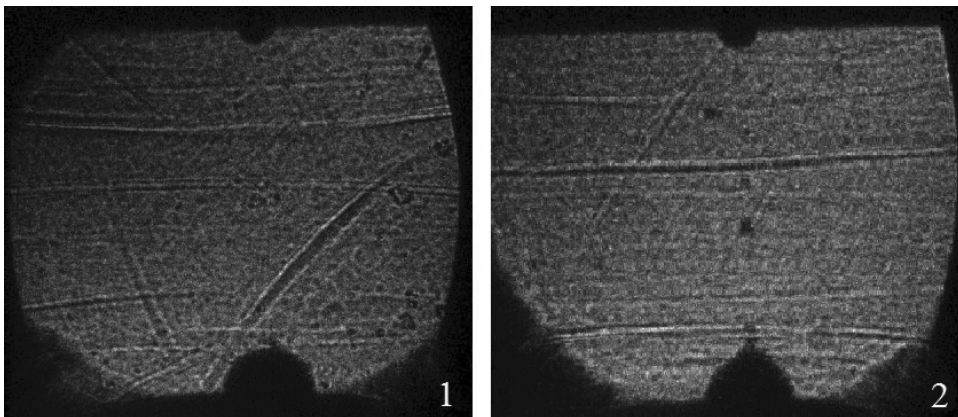


Figure 11. Cavitation bubbles at the same time delay (t = 50 µs). 1) In non-degassed deionized water. 2) In degassed deionized water. In both cases the thickness of the water layer was 5 mm.

## Acknowledgements

## References

[1] A. Kruusing, Handbook of liquids-assisted laser processing, Elsevier, 464p. 2007.

[2] J. L. Ocaña, C. Molpeceres, J. A. Porro, G. Gómez, and M. Morales, "Experimental assessment of the influence of irradiation parameters on surface deformation and residual stresses in laser shock processed metallic alloys," Applied Surface Science 238, 501-505 (2004).

[3] G. Gómez-Rosas, C. Rubio-González, J. L. Ocaña, C. Molpeceres, J. A. Porro, W. Chi-Moreno, and M. Morales, "High level compressive residual stresses produced in aluminum alloys by laser shock processing," Applied Surface Science 252, 883-887 (2005).

[4] G. W. Yang, "Laser ablation in liquids: Application in the synthesis of nanocrystals," J. Phys. Chem. B 52, 647-698 (2007).

[5] D. Song, M. H. Hong, B. Lukyanchuk, and T. C. Chong, "Laser-induced cavitation bubbles for cleaning of solid surfaces," J Appl. Phys. 95, 2952-2956 (2004).

[6] R. O. Esenaliev, A. A. Oraevsky, V. S. Letokhov, A. A. Karabutov, and T. V. Malinsky, "Studies of acoustical and shock waves in the pulsed laser ablation of biotissue," Lasers Surg. Med. 3, 470-484 (1993).

[7] P. K. Kennedy, D. X. Hammer, and B. A. Rockwell, "Laser-induced breakdown in aqueous media," Prog. Quant. Electr. 21, 155-248 (1997).

[8] J. L. Ocaña, M. Morales, C. Molpeceres, J. Torres, J.A. Porro, G. Gómez, and C. Rubio, "Predictive assessment and experimental characterization of the influence of irradiation parameters on surface deformation and residual stresses in laser shock processed metallic alloys," High-Power Laser Ablation IV, Phipps C.R., Ed., SPIE 5548, 642-653 (2004).

[9] A. Vogel and W. Lauterborn, "Acoustic transient generation by laser-produced cavitation bubbles near solid boundaries," J. Acoust. Soc. Amer. 84, 719-731 (1988).

[10] M. S. Plesset and R.B. Chapman, "Collapse of an initially spherical vapour cavity in the neighbourhood of a solid boundary," J. Fluid Mech. 47, 283-290 (1971).

[11] A. Philipp and W. Lauterborn, "Cavitation erosion by single laser-produced bubbles," J. Fluid. Mech. 361, 75-116 (1998).

[12] J. P. Chen, X. W. Ni, J. Lu, B. M. Bian, and Y. W. Wang, "Laser-induced plasma shock wave and cavity on metal surface underwater," Microwave and Optical Technology Letters 25, 307-311 (2000).

[13] Xiao Chen, Rong-Qing Xu, Jian-Ping Chen, Zhong-Hua Shen, Lu Jian, and Xiao-Wu Ni, "Shock-wave propagation and cavitation bubble oscillation by Nd:YAG laser ablation of a metal in water," Appl. Opt. 43, 3251-3257 (2004).

[14] S. Suzuki, T. Itoh, and D. Suzuki, "Visualization and pressure measurement of underwater shock waves induced by pulsed laser irradiation," Symposium on Interdisciplinary Shock Wave Research, Sendai, Japan. March 22-24, 2004. Available at http://rainbow.ifs.tohoku.ac.jp/~iswi/ISISW/ISISWsuzuki.pdf. Last accessed on December 9, 2008.3.

[15] J. Lubbers and R. Graaff, "A simple and accurate formula for the sound velocity in water," Ultrasound Med. Biol. 24, 1065–1068 (1998)

[16] L. Marti-Lopez, R. Ocaña, J. Porro. M. Morales and J.L. Ocaña, "Optical observation of shock waves and cavitation bubbles in high intensity laser induced shock processes" Applied Optics 48, 3671(2009)

[17] F.Docchio, P.Regondi, M.R.C.Capon, J.Mellerio, "Study of the temporal and special dynamics of plasmas induced in liquids by nanosecond Nd:YAG laser pulses. 1: Analysis ofthe plasma starting times," Applied Optics; vol. 27 no. 17; 1 September 1988; pp 3661-3667.

[18] R. P. Taleyarkhan, C. D. West, J. S. Cho, R. T. Lahey Jr., R. I. Nigmatulin, R. C. Block, "Evidence for Nuclear Emissions During Acoustic Cavitation", SCIENCE vol 295 pp1868-1873.